JOURNAL OF MATERIALS SCIENCE 22 (1987) 4274-4280

Phase equilibria and thermodynamic properties in the system Ni–Mo–O

K. T. JACOB, G. M. KALE, G. N. K. IYENGAR
Department of Metallurgy, Indian Institute of Science, Bangalore 560 012, India

Coexisting phases in the Ni–Mo–O ternary system at 1373 K have been identified by X-ray diffraction, optical microscopy and scanning electron microscopy. The samples were equilibrated in evacuated quartz capsules. Only one ternary phase, $NiMoO_4$, was found to exist in the system. The reversible e.m.f. values of the following solid-state galvanic cells were measured in the temperature range 900 to 1500 K: (I) Pt, Ni + NiO/(CaO) ZrO_2/NiO + MoO_2 + $NiMoO_4$, Pt; (II) Pt, Mo + MoO_2/(CaO) ZrO_2/O_2, Pt; and (III) Pt, Mo + MoO_2/(CaO) ZrO_2/Ni–Mo + MoO_2, Pt. The Gibbs energies of formation of $NiMoO_4$ and MoO_2 and activities in Ni–Mo alloys were derived from the e.m.f. data. For the reaction $\langle NiO\rangle + \langle MoO_2\rangle + \frac{1}{2}(O_2) \rightarrow \langle NiMoO_4\rangle$ we obtain $\Delta G_r^0 = -201\,195 + 69.70T\ (\pm 400)\ J\,mol^{-1}$; for $\langle Mo\rangle + (O_2) \rightarrow \langle MoO_2\rangle$ we obtain $\Delta G_f^0 = -578\,880 + 168.5T\ (\pm 500)\ J\,mol^{-1}$. Based on the information from phase identification studies and thermodynamic stabilities, the isothermal section and oxygen potential diagram for the Ni–Mo–O system at 1373 K have been developed.

1. Introduction

Among nickel-based superalloys, those of the Ni–Mo series are known for their ability to withstand corrosion at high temperatures. Hastelloys (Union Carbide Corp., USA) constitute an important group of the Ni–Mo series extensively used as high temperature materials. Hastelloy B is used up to 950 K in oxidizing atmospheres, whereas Hastelloy X has excellent strength and corrosion resistance up to 1400 K [1, 2]. Phase diagrams are useful for assessing the stability of alloys in corrosive atmospheres at elevated temperatures. Since phase diagram determination for complex alloys is expensive and time-consuming, efforts have been directed at computer calculation of phase diagrams from the basic thermodynamic properties of binary systems. This procedure, however, will not predict the presence of ternary or higher-order compounds. Information on such phases must be provided independently for the generation of multicomponent phase diagrams.

Although the phase diagrams and thermodynamic properties of three binaries constituting the Ni–Mo–O ternary system are relatively well established, information on ternary phase relations is not available in the literature. In the Ni–O binary the only stable oxide at high temperature and ambient pressure is NiO [3]. The thermodynamic data for NiO are well established [4]. As discussed by Brewer *et al.* [5], there are a number of oxides that are stable at low temperatures in the Mo–O system. However, at 1373 K the stable phases are solid "MoO_2" and liquid "MoO_3", both of which are non-stoichiometric. Numerous investigations have been reported in the literature [5–19] on the thermodynamic properties of MoO_2 using gas equilibration techniques [6, 7], e.m.f. methods [8–18] and calorimetry [19]. In spite of so many investigations, minor discrepancies still exist in the thermodynamic data for MoO_2, as pointed out in a recent review by Brewer *et al.* [5]. The phase diagram of the Ni–Mo system [5] shows that in the solid state Ni(fcc) exhibits negligible solubility in Mo(bcc), but molybdenum is soluble in nickel. At 1373 K the terminal solid solubility in the fcc phase extends up to 24 at % Mo. Further, three intermetallic compounds, MoNi, $MoNi_3$ and $MoNi_4$, which are stable up to 1592, 1183 and 1143 K, respectively, have been identified in this system. The metastable phases $MoNi_2$, $MoNi_3$ and Mo_5Ni_{17} have also been reported [5].

Thermodynamic data on Ni–Mo alloys up to 1967 has been reviewed by Hultgren *et al.* [20]. In addition Spencer and Putland [21] have measured the high-temperature heat capacity (773 to 1573 K) and enthalpy of formation (973 to 1573 K) for $Ni_{0.48}Mo_{0.52}$. The enthalpy of formation was found to be temperature-dependent, varying from $-1000\ J\,mol^{-1}$ at 973 K to $750\ J\,mol^{-1}$ at 1573 K. E.m.f. measurements on activities in the Ni–Mo system were reported by Meshkov *et al.* [22] (1073 to 1348 K; $0.03 \leqslant X_{Mo} \leqslant 0.40$) and Katayama *et al.* [23] (1223 to 1373 K; $0.05 \leqslant X_{Mo} \leqslant 0.75$). Results of the two e.m.f. studies and the calorimetric measurements are not entirely consistent. Kaufman and Nesor [24] and Brewer *et al.* [5] have evaluated thermodynamic data for this system.

2. Experimental procedure

2.1. Scope

Phase relations in the Ni–Mo–O system at 1373 K were studied by equilibrating mixtures of metal/alloy and oxides in evacuated quartz capsules. The equilibrium phases were identified by metallography and X-ray diffraction. The free energies of formation of binary and ternary oxides and the activities in the alloy phase were determined using solid-state galvanic

0022–2461/87 $03.00 + .12 © *1987 Chapman and Hall Ltd.*

cells. From these measurements the isothermal section of Ni–Mo–O phase diagram at 1373 K was composed. The oxygen potentials for univariant and bivariant equilibria in the ternary system were computed from the thermodynamic data obtained from e.m.f. measurements.

2.2. Materials

Fine powders of molybdenum, molybdenum trioxide, nickel and nickel oxide were obtained from Fischer Scientific Co., USA. The molybdenum dioxide (MoO_2) was prepared by reacting the mixture (Mo + MoO_3) at 1373 K for 24 h in an evacuated quartz capsule. The compound $NiMoO_4$ was prepared by mixing fine powders of NiO and MoO_2, pelletizing the mixture and heating in air at 1473 K for 40 h. X-ray diffraction showed that the structure was monoclinic with a = 0.960 nm, b = 0.874 nm, c = 0.771 nm and β = 113.4°. Attempts to prepare the compound $Ni_2Mo_3O_8$ ($2NiO \cdot 3MoO_2$) from component oxides were unsuccessful. The argon gas used in e.m.f. measurements was 99.99% pure. It was dried by passing through magnesium perchlorate and deoxidized by copper turnings held at 723 K and titanium granules at 1073 K. Calcia-stabilized zirconia solid electrolyte tubes were obtained from Corning Glass Works (Corning, USA). The Ni–Mo alloys were prepared in a small arc furnace with water-cooled copper electrodes.

2.3. Apparatus and procedure

2.3.1. Phase relations

Fine powders of metal and oxides, taken in appropriate molar ratios, were thoroughly mixed in a ball mill and pressed into pellets of 5 mm diameter and 2.5 mm thickness. The initial compositions of pellets are given in Table I. The pellets were contained in small alumina crucibles which were sealed inside evacuated quartz capsules. Several capsules were kept in the muffle furnace maintained at 1373(±2) K for 168 h to ensure the attainment of thermodynamic equilibrium. Preliminary experiments had indicated that approximately 120 h are sufficient for the attainment of equilibrium. The alloys used in these experiments were pre-equilibrated in evacuated quartz capsules for 120 h and then mixed with oxides for further equilibration. After equilibration, the samples were quenched in liquid nitrogen and the phases present were identified by X-ray diffraction, optical microscopy and scanning electron microscopy. The alloy compositions were determined by energy-dispersive analysis of X-rays (EDAX), using pure metals as standards.

2.3.2. E.m.f. measurements

The e.m.f. values of the following three galvanic cells incorporating calcia-stabilized zirconia as solid electrolyte were measured:

$$\text{Pt, Ni} + \text{NiO}/(\text{CaO})\text{ZrO}_2/\text{NiO} + \text{MoO}_2 + \text{NiMoO}_4, \text{Pt} \quad \text{(I)}$$

$$\text{Pt, Mo} + \text{MoO}_2/(\text{CaO})\text{ZrO}_2/\text{O}_2, \text{Pt} \quad \text{(II)}$$

$$\text{Pt, Mo} + \text{MoO}_2/(\text{CaO})\text{ZrO}_2/\text{Ni–Mo} + \text{MoO}_2, \text{Pt} \quad \text{(III)}$$

The cells are written such that the right-hand electrode is positive. The e.m.f. values of Cells I and II were measured in the temperature range 900 to 1500 K, while the e.m.f. of Cell III was measured only at 1373 K. The apparatus used for e.m.f. measurements on Cells I and II was similar to that described earlier [25]. The solid electrodes were prepared in the form of pellets by compacting an intimate equimolar mixture of component phases and subsequent sintering in evacuated quartz capsules. The flat surfaces of pellets were polished and spring-loaded against both sides of the flat-ended $(CaO)ZrO_2$ tube. Independent streams of argon gas were passed over the solid electrodes in Cell I at flow rates between 100 and 300 ml min^{-1}. In the case of the oxygen electrode in Cell II, pure oxygen was passed at a flow rate between 100 and 200 ml min^{-1} and a pressure of 1.01×10^5 Pa. The pressure was controlled by having a mercury bubbler at the gas exit, whose height was adjusted periodically in response to barometric changes. A schematic diagram of Cell III is shown in Fig. 1. The electrode mixture was covered with a layer of dry alumina powder to minimize interaction with the gas phase. Each electrode was flushed with a separate stream of purified argon gas. The e.m.f. was measured by a digital voltmeter with an internal impedance greater than $10^{12}\ \Omega$.

In one experiment a symmetric cell with (Ni + NiO) electrodes on both sides of the solid electrolyte was set up. The e.m.f. of the cell was ±0.1 mV, with

TABLE I Equilibrium phases in different regions of the Ni–Mo–O system at 1373 K, identified by X-ray diffraction, optical microscopy and scanning electron microscopy

Composition of pellets before equilibration (molar ratios)	Phases present after equilibration at 1373 K
$2MoO_3 + MoO_2 + NiO$	$NiMoO_4 + MoO_2 + MoO_3$ (l)
$MoO_3 + 2Ni$	$Ni + NiO + MoO_2$
$NiMoO_4 + 3Ni$	$Ni + NiO + MoO_2$
$1.75\,MoO_3 + NiO + 0.75\,Ni$	$NiO + NiMoO_4 + MoO_2$
$MoO_2 + 0.73\,Mo + 0.27\,Ni^*$	$MoO_2 + Mo_{ss}(bcc) + MoNi$
$MoO_2 + 0.37\,Mo + 0.63\,Ni^*$	$MoO_2 + MoNi + Mo_{0.24}Ni_{0.76}(fcc)$
$MoO_2 + Mo_{0.23}Ni^*_{0.77}$	$MoO_2 + Mo_{0.23}Ni_{0.27}(fcc)$
$MoO_2 + Mo_{0.15}Ni^*_{0.85}$	$MoO_2 + Mo_{0.15}Ni_{0.85}(fcc)$
$MoO_2 + Mo_{0.094}Ni^*_{0.906}$	$MoO_2 + Mo_{0.094}Ni_{0.906}(fcc)$
$MoO_2 + Mo_{0.045}Ni^*_{0.955}$	$MoO_2 + Mo_{0.045}Ni_{0.955}(fcc)$
$1.5\,NiO + Mo_{0.23}Ni^*_{0.77}$	$MoO_2 + NiO + Ni(fcc)$

*The alloy was pre-equilibrated.

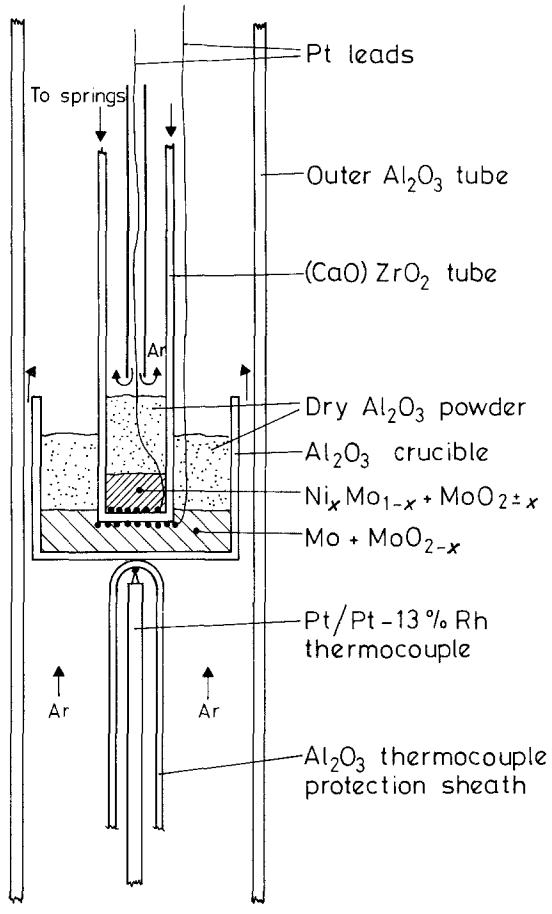

Figure 1 Schematic diagram of the apparatus for e.m.f. measurements on Cell III.

no systematic temperature dependence, indicating that thermoelectric contributions are negligible. The reversibility of the e.m.f. was checked by passing small currents ($\sim 100\,\mu A$) through the cell for approximately 3 min in either direction. In each case the e.m.f. was found to return to the steady-state value before the titration in 15 min. The e.m.f. was also independent of the flow rate of gases and reproducible on temperature-cycling. The time required for obtaining steady e.m.f. values varied from 2 to 8 h depending on the composition of the electrode and the temperature. At the end of the experiment the solid electrodes were examined by X-ray diffraction and optical microscopy. Apart from the sintering of particles, no other change was detected. The composition of the electrodes was not altered during the e.m.f. measurements.

3. Results and discussion

3.1. Phase diagram

The phases identified after equilibration of various condensed phase mixtures in silica capsules are summarized in Table I. At 1373 K there is only one intermetallic compound of variable composition in the Ni–Mo system. The maximum solubility of molybdenum in fcc nickel was found to be 24 at %, in good agreement with the literature [5]. Only one ternary oxide, $NiMoO_4$, has been identified in this study. A section of the ternary phase diagram of the Ni–Mo–O system at 1373 K and total pressure of 1.01×10^5 Pa, constructed from the results of the present study, is shown in Fig. 2. The overall compositions of the samples used in phase identification studies are shown by symbols on the diagram, the circles representing samples which contained two condensed phases and triangles representing compositions in the three-phase fields. The diagram is consistent with the information available in the literature on the constituent binaries [4, 5]. There are five three-phase fields involving condensed phases. The oxygen partial pressures over these three-phase mixtures are uniquely

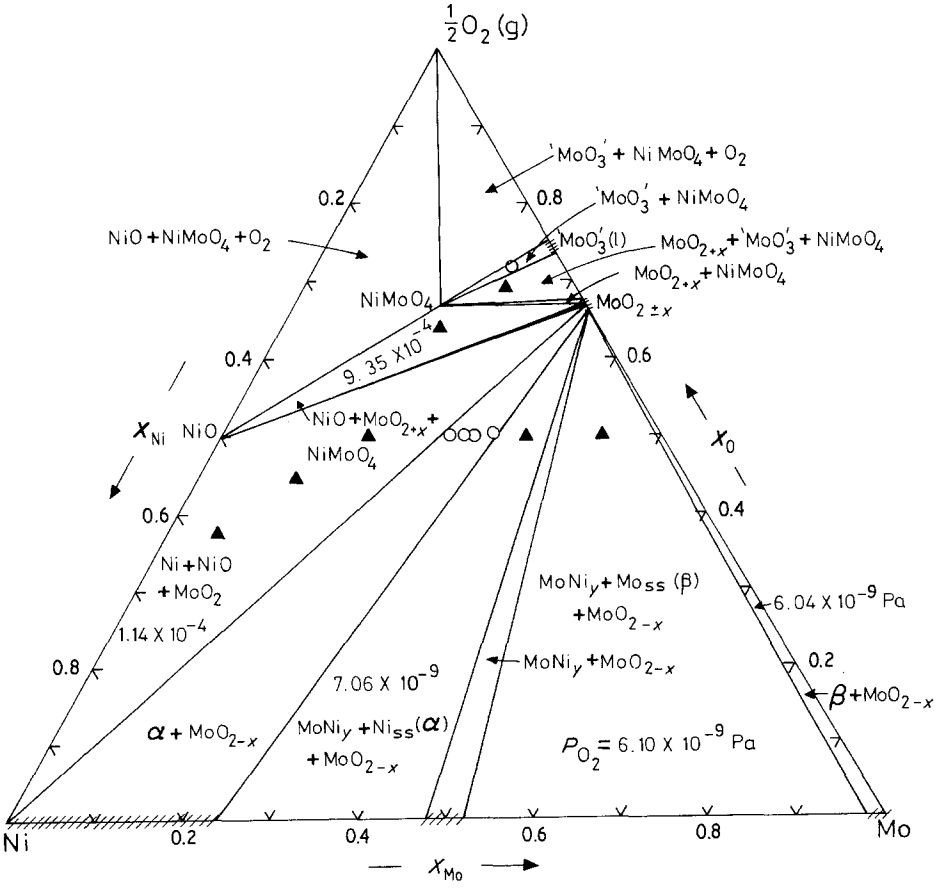

Figure 2 Isothermal section of Ni–Mo–O system at 1373 K. The overall compositions of samples used for phase identification are shown: (▲) Samples containing three phases, (○) two-phase mixtures.

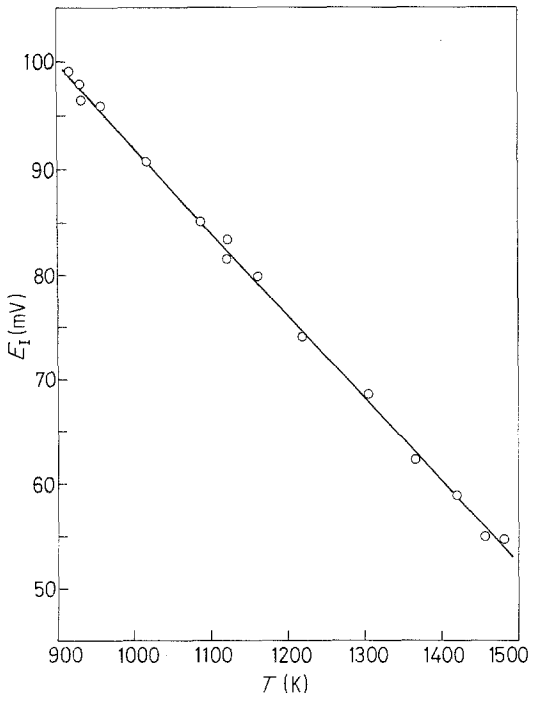

Figure 3 Variation of the e.m.f. of Cell I with temperature. E_I = 170.8 − 0.0788T mV.

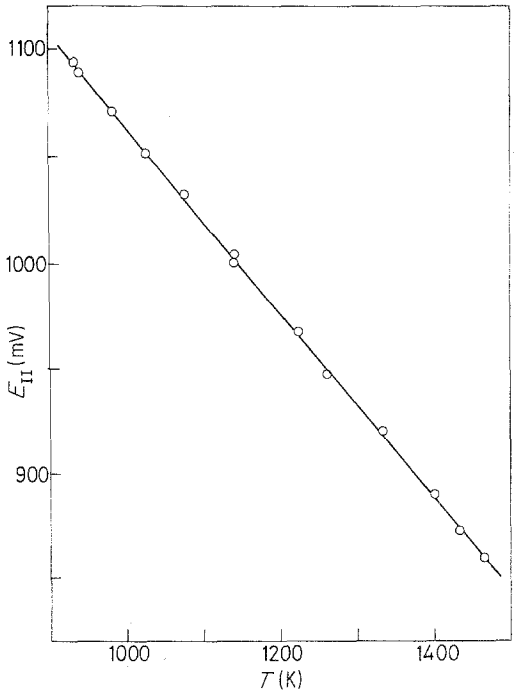

Figure 4 Temperature dependence of the e.m.f. of Cell II. E_{II} = 1499.8 − 0.4365T (±1.3) mV.

defined at each temperature and are indicated in Fig. 2. The variation of oxygen potential with composition is discussed in Section 3.4. There is no evidence of the compound $2NiO \cdot 3MoO_2$ reported earlier [26]. The two-phase fields $NiMoO_4 + O_2$, $NiO + NiMoO_4$, $NiO + MoO_2$ and the homogeneity range of compounds NiO and $NiMoO_4$ are too narrow to be shown on the ternary Ni–Mo–O phase diagram at 1373 K.

3.2. Oxygen potentials and Gibbs energies

The temperature dependence of the e.m.f. of Cells I and II is shown in Figs 3 and 4, respectively. The e.m.f. varies linearly with temperature. The least-squares regression analysis yields

$$E_I = 170.8 - 0.0788T(\pm 0.8)\,\text{mV} \quad (1)$$

and

$$E_{II} = 1499.8 - 0.4365T(\pm 1.3)\,\text{mV} \quad (2)$$

The e.m.f. is related to the difference in oxygen potential between the electrodes

$$\eta F E_I = \Delta\mu_{O_2(NiO+MoO_2+NiMoO_4)} - \Delta\mu_{O_2(Ni+NiO)} \quad (3)$$

$$\eta F E_{II} = \Delta\mu_{O_2(Mo+MoO_2)} \quad (4)$$

where η (=4) is the number of electrons associated with the electrode reaction and F is the Faraday constant. The oxygen potential of the (Ni + NiO) reference electrode is taken from Steele [4]:

$$\Delta\mu_{O_2(Ni+NiO)} = -468\,315 + 169.8T\,\text{J mol}^{-1} \quad (5)$$

The oxygen potential of the right-hand electrode in Cell I, computed from the e.m.f., is defined by

$$2NiO(s) + 2MoO_2(s) + O_2(g) \rightarrow 2NiMoO_4(s) \quad (6)$$

$$\Delta G_r^0 = \Delta\mu_{O_2} = -402\,390 + 139.39T(\pm 800)\,\text{J mol}^{-1} \quad (7)$$

For the reaction

$$Mo(s) + O_2(g) \rightarrow MoO_2(s) \quad (8)$$

the e.m.f. of Cell II gives

$$\Delta G_f^0 = \Delta\mu_{O_2} = -578\,880 + 168.5T(\pm 500)\,\text{J mol}^{-1} \quad (9)$$

The uncertainty estimates are based on twice the standard deviation and on errors in the chemical potentials of the reference electrodes. The Gibbs energy of formation of $NiMoO_4$ from the component solid oxides is obtained by combining Equations 7 and 9 with the standard free energy of formation of MoO_3(s) in the literature [5, 27]. For the reaction

$$NiO(s) + MoO_3(s) \rightarrow NiMoO_4(s) \quad (10)$$

we obtain

$$\Delta G^0 = -49\,915 - 0.01T(\pm 1000)\,\text{J mol}^{-1} \quad (11)$$

The "second law" enthalpy of formation of $NiMoO_4$ from component oxides in the solid state is −49.9 (±3.5) kJ mol^{-1}. This is of the same magnitude as the enthalpy of formation of a similar compound, $NiWO_4$, ($\Delta H^0 = -44\,\text{kJ mol}^{-1}$) reported by Jacob [28] using an identical e.m.f. technique. Calorimetric measurements of the enthalpy of formation of $NiMoO_4$ are not available for comparison. The free energy of formation of $NiMoO_4$ from elements is obtained by combining Equations 5, 7 and 9. For the reaction

$$Ni(s) + Mo(s) + 2O_2(g) \rightarrow NiMoO_4(s) \quad (12)$$

we obtain

$$\Delta G^0 = -1\,014\,230 + 323.1T(\pm 1200)\,\text{J mol}^{-1} \quad (13)$$

The standard Gibbs energy of formation of MoO_2 obtained in this study is compared with data reported

TABLE II Comparison of Gibbs energy of formation of $\langle MoO_2 \rangle$

Author/s	Technique	Temperature range (K)	$-\Delta G_f^0$ for $\langle MoO_2 \rangle$ (kJ mol^{-1})			
			900 K	1100 K	1300 K	1500 K
Gokcen [6]	H_2/H_2O	950 to 1350	–	391.6	362.2	–
Gleiser and Chipman [7]	CO/CO_2	1200 to 1350	–	–	358.4	–
Rapp [8]	e.m.f.	1023 to 1323	–	391.6	358.2	–
Barbi [9]	e.m.f.	873 to 1073	418.66	383.06	–	–
McIver and Teale [10]	e.m.f.	1115 to 1280	–	339.1	304.3	–
Dorbyshev *et al.* [11]	e.m.f.	1280 to 1360	–	–	355.4	–
Iordanov *et al.* [12]	e.m.f.	973 to 1123	–	393.3	–	–
Berglund and Kierkegaard [13]	e.m.f.	1150 to 1450	–	–	355.49	–
Alcock and Chan [14]	e.m.f.	1273 to 1873	–	–	362.33	328.9
Chastant *et al.* [15]	e.m.f.	1073 to 1673	–	392.5	357.04	321.6
Chattopadhyay *et al.* [16]	e.m.f.	1040 to 1290	–	388.52	356.22	–
Iwase *et al.* [17]	e.m.f.	1273 to 1723	–	–	356.14	322.3
Katayama and Kozuka [18]	e.m.f.	903 to 1540	–	390.03	356.23	322.56
King *et al.* [19]	Calorimetry		425.4	391.41	357.4	323.4
Brewer *et al.* [5] and JANAF [30] for O_2	Evaluation	800 to 1500	422.78	388.76	354.74	320.72
Present study	e.m.f.	900 to 1500	427.33	393.53	359.83	326.13

in the literature in Table II. The results of this study are in good agreement with the gas equilibrium measurements of Gokcen [6] and Gleiser and Chipman [7], the e.m.f. measurements of Rapp [8], Iordonov *et al.* [12] and Alcock and Chan [14], and the calorimetric data of King *et al.* [19]. The data of Chastant *et al.* [15] agree well with the present results at lower temperatures but diverge at higher temperatures. The e.m.f. results of Dorbyshev *et al.* [11], Berglund and Kierkegaard [13], Chattopadhyay *et al.* [16] and Iwase *et al.* [17] and the evaluated data of Brewer *et al.* are 3.5 to 5.5 kJ mol^{-1} more positive than the results obtained in this study. The data of Barbi [9] and McIver and Teale [10] are not compatible with the results of this study.

There is significant difference between the entropy values given for MoO_2 by Brewer *et al.* [5] and the JANAF data [27]. Molybdenum dioxide has a deformed rutile-type structure in which each molybdenum atom is coordinated by six oxygen atoms to form MoO_6 octahedra. The octahedra are joined by sharing edges to form strings which are mutually connected into a three-dimensional structure by corner-sharing of the octahedra. In the ideal rutile structure, the metal atoms are equidistant within the strings, but in the MoO_2 structure the metal–metal distances are alternately short (0.251 nm) and long (0.311 nm). This results in the formation of pairs of metal atoms and consequent distortion of the MoO_6 octahedra, which lowers the symmetry from tetragonal for rutile to monoclinic for MoO_2. Heat capacity measurements on MoO_2 extend only down to 51 K. JANAF evaluation [27] has considered the possibility that MoO_2 is antiferromagnetic at low temperature and has anticipated enhanced heat capacity below 50 K, owing to spin interactions of unpaired electrons. However, Ghose *et al.* [29] have shown the absence of permanent magnetic moment in MoO_2 by neutron diffraction. In MoO_2 the two 4d electrons of molybdenum are in t_{2g} orbitals. These overlap along the *c* axis, i.e. d_{xy} and d_{yz}, forming metal–metal double bonds. The small magnetic moment of Mo(IV) is due to Pauli paramagnetism arising from the collective electrons in the overlapping Mo–O π^* band, which itself is similar in energy to the Mo–Mo σ and π bonds. Brewer *et al.* [5] do not therefore consider additional contributions to S_{51}^0.

The "third law" analysis of the Gibbs energy of formation of MoO_2 obtained in this study using the free energy functions for molybdenum and MoO_2 from Brewer *et al.* [5] and for O_2 from JANAF tables [30] yields ΔH_f^0 (298.15 K) = -592.8 (± 0.9) kJ mol^{-1}. This value is 5.0 kJ mol^{-1} more negative than that recommended by Brewer *et al.* [5] and JANAF tables [27].

3.3. Activities in Ni–Mo alloys

The e.m.f. of Cell III is shown in Fig. 5 as a function of alloy composition at 1373 K. The e.m.f. is related to the activity of molybdenum in the oxygen saturated alloy by

$$-\eta F E_{III} = RT \ln a_{Mo} \quad (14)$$

Since the solubility of oxygen in the solid alloy is negligible, the activities along the oxygen-saturated

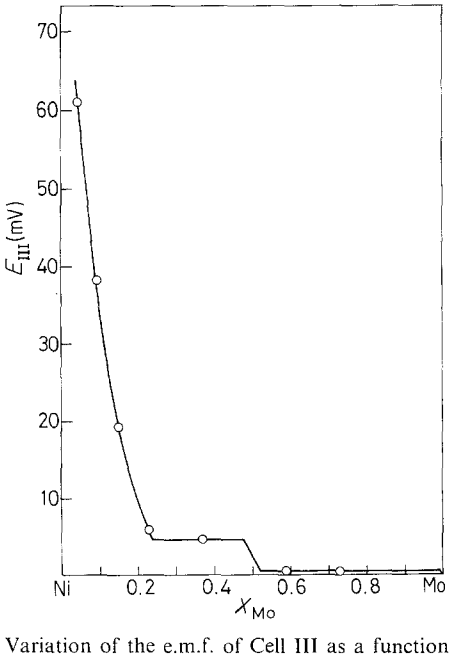

Figure 5 Variation of the e.m.f. of Cell III as a function of alloy composition at 1373 K.

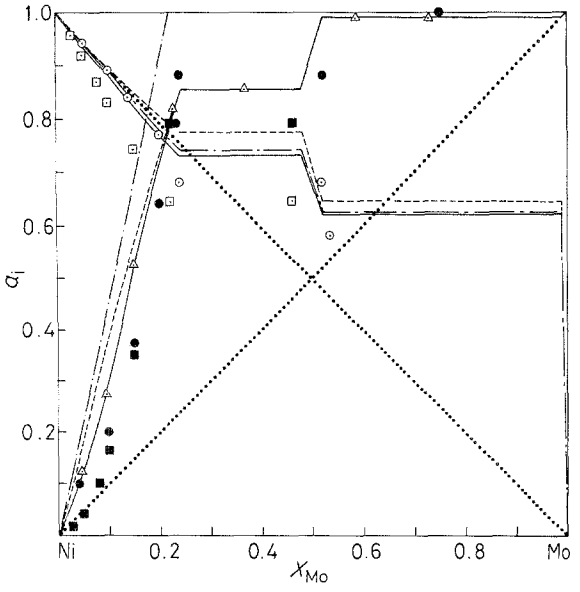

Figure 6 Activity–composition relations in Ni–Mo system at 1373 K. (– · · · –) Brewer *et al.* [5]; (– – –) Kaufman and Nesor [24]; (●, ⊙) Katayama *et al.* [23]; (■, ⊡) Meshkov *et al.* [22]; (△, ——) this work.

boundary can be considered to be the same as that in the binary Ni–Mo system. The activity–composition relationship for the binary system at 1373 K is shown in Fig. 6. The activity of nickel is derived using the Gibbs–Duhem equation and is consistent with the phase diagram [5]. The values obtained in earlier e.m.f. studies and those suggested in recent evaluations are also shown in the figure for comparison. The activity of molybdenum in dilute solution in fcc nickel obtained in this study is significantly higher than that obtained by Meshkov *et al.* [22] and Katayama *et al.* [23]. At higher concentrations of molybdenum the activity obtained in this study falls between the values obtained in the earlier studies. The measurements of Meshkov *et al.* [22] cover the temperature range 1073 to 1364 K, and have been extrapolated to 1373 K for comparison. Surface depletion of molybdenum due to the oxidation of alloy powder by residual oxygen in the inert gas can result in low activity values, especially for dilute alloys.

There appears to be a printing mistake in the equation for the activity coefficient of molybdenum in fcc nickel given in the recent evaluation by Brewer *et al.* [5]: the activity calculated from their equation is greater than unity for $X_{Mo} > 0.22$. The values for the activity of nickel given by Brewer *et al.* [5] are in reasonable agreement with the data obtained in this study.

Kaufman and Nesor [24] have given algebraic expressions for the thermodynamic properties of all phases in the Ni–Mo system, and these generate a phase diagram resembling that obtained by experiment. These equations, combined with lattice stabilities for nickel [31, 32], can be used to derive the activities. Their values for molybdenum are in good overall agreement with the results of this study. The activity of nickel suggested by Kaufman and Nesor [24, 31, 32] is slightly higher than that obtained in this study.

The free energy of formation of the $MoNi_y$ phase calculated from the results of this study is $-5.29\ (\pm 0.2)\,kJ\,mol^{-1}$ at 1373 K, independent of stoichiometry. The corresponding values from the e.m.f. studies of Meshkov *et al.* [22] and Katayama *et al.* [23] are -7.48 and $-6.23\,kJ\,mol^{-1}$, respectively. Calorimetric measurements [21] give a slightly positive heat of mixing at 1373 K, and can be reconciled with the results of this study only by assuming

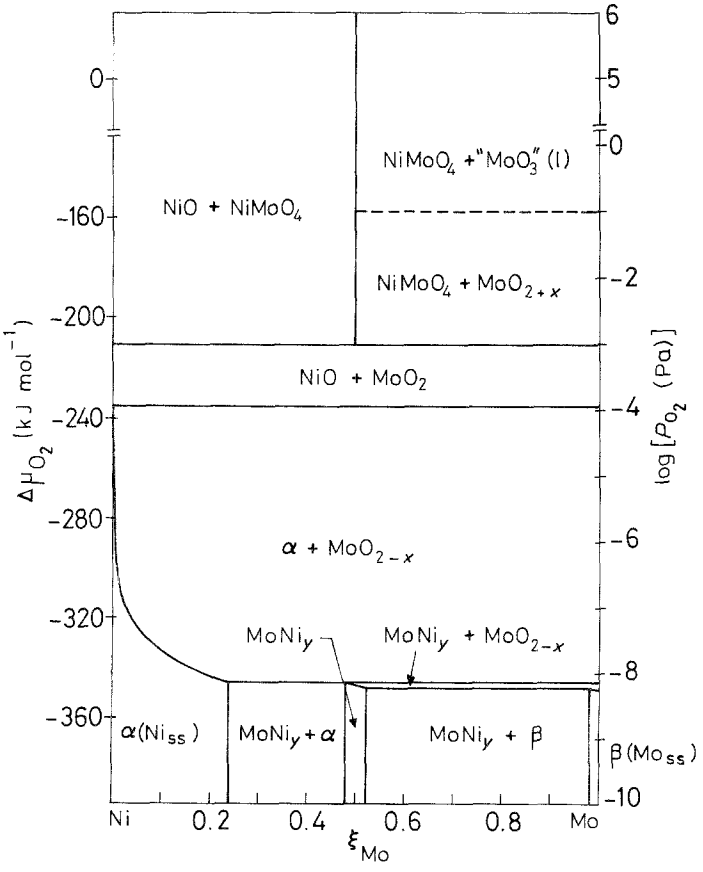

Figure 7 Oxygen potential–composition diagram for the Ni–Mo–O system at 1373 K.

a significantly positive entropy of formation. It is more likely, however, that the calorimetric values are affected by the vaporization of the alloy at high temperatures. The vaporization effects become more significant with increasing temperature, and perhaps account for the increasing endothermicity of alloy formation with temperature [21]. The enthalpies of formation of alloys in Co–Cr and Mo–Cr systems obtained by using the same adiabatic calorimeter have also been found recently to be too endothermic [33, 34].

3.4. Oxygen potential–composition diagram

The variation of oxygen potential with the mole ratio $\xi_{Mo} = n_{Mo}/(n_{Mo} + n_{Ni})$ where n = no. of moles, in the Ni–Mo–O system at 1373 K and a total pressure of 1.01×10^5 Pa, is shown in Fig. 7. The composition variable ξ_{Mo} is defined such that it is independent of the moles of oxygen. This diagram is more useful for the interpretation of high-temperature corrosion behaviour than the conventional Gibbs ternary representation (Fig. 2). The oxidation product at any specific oxygen partial pressure and alloy composition can be readily identified using Fig. 7. The main disadvantage of the oxygen potential–composition diagram is its inability to depict oxygen nonstoichiometry. The three-phase equilibria are shown as horizontal lines in Fig. 7. The oxygen potential variations with composition in the two-phase regions (α + MoO_{2-x}), ($MoNi_y$ + MoO_{2-x}) and (β + MoO_{2-x}) are calculated from the Gibbs energy of formation of MoO_2 and the activities in Ni–Mo alloys. At $P_{O_2} > 9.4 \times 10^{-4}$ Pa, $NiMoO_4$ is stable in the Ni–Mo–O system at 1373 K. However, $NiMoO_4$ is never in equilibrium with Ni–Mo alloys. It is formed only by the oxidation of (NiO + MoO_2) mixtures or by reaction between NiO and MoO_3. The oxygen potential for the oxidation of solid MoO_2 to liquid "MoO_3" is calculated from the evaluated data of Brewer *et al.* [5] and requires further confirmation by experiment. Oxygen potential–composition diagrams at other temperatures can be easily calculated from the thermodynamic data reported in this study.

Acknowledgements

The authors are grateful to Shri N. Venugopal Rao and Shri A.V. Narayan for help in preparation of the manuscript.

References

1. J. L. EVERHART, "Engineering Properties of Nickel and Nickel Alloys" (Plenum, New York, 1971) p. 46.
2. C. T. SIMS and W. C. HEGEL, "The Superalloys" (Wiley, New York, 1972) p. 8.
3. E. M. LEVIN, C. R. ROBBINS and H. F. McMURDIE, "Phase Diagrams for Ceramists" (American Ceramic Society, Columbus, Ohio, 1964) p. 40.
4. B. C. H. STEELE, in "Electromotive Force Measurements in High Temperature Systems", edited by C. B. Alcock (Institute of Mining and Metallurgy, London, 1968) p. 21.
5. L. BREWER, R. H. LAMOREAUX, R. FERRO, R. MARAZZA and K. GIRGIS, "Molybdenum: Physicochemical Properties of its Compounds and Alloys" (Atomic Energy Review Agency, Vienna, 1980) pp. 30–285.
6. N. A. GOCKEN, *Trans. AIME* **197** (1953) 1019.
7. M. GLEISER and J. CHIPMAN, *J. Phys. Chem.* **66** (1962) 1539.
8. R. A. RAPP, *Trans. Met. Soc. AIME* **227** (1963) 371.
9. G. B. BARBI, *J. Phys. Chem.* **68** (1964) 1025.
10. E. J. McIVER and S. S. TEALE, UKAEA Research Group, Harwell, Atomic Energy Establishment Report, AERE-R 4942 (1965) p. 17.
11. V. N. DORBYSHEV, T. N. REZUKHINA and L. A. TARASOVA, *Russ. J. Phys. Chem.* **39** (1965) 70.
12. K. V. IORDANOV, T. G. NIKOLOV and M. T. CHIMBULEV, *Neue Huette* **13** (1968) 215.
13. S. BEGLUND and P. KIERKEGAARD, *Acta Chem. Scand.* **23** (1969) 329.
14. C. B. ALCOCK and J. C. CHAN, *Can. Met. Quart.* **11** (1972) 559.
15. M. CHASTANT, C. GATELLIER, M. M. JON and M. OLETTE, *Rep. IRSID* **138** (1973) 951.
16. G. CHATTOPADHYAY, S. N. TRIPATHI and A. S. KERKAR, *J. Amer. Ceram. Soc.* **67** (1984) 610.
17. M. IWASE, M. YASUDA and T. MORI, *Electrochim. Acta* **24** (1979) 261.
18. I. KATAYAMA and Z. KOZUKA, *Tech. Rep. Osaka Univ.* **23** (1973) 411.
19. E. G. KING, W. W. WELLER and A. U. CHRISTENSEN, US Bur. Min. Rep. Invest. No. 5664 (US Bureau of Mines, Washington, D.C., 1960) p. 29.
20. R. HULTGREN, P. D. DESAI, D. T. HAWKINS, M. GLEISER and K. K. KELLEY, "Selected values of the Thermodynamic Properties of Binary Alloys" (American Society for Metals, Metals Park, Ohio, 1973) p. 1145.
21. P. J. SPENCER and F. H. PUTLAND, *J. Chem. Thermodyn.* 7 (1975) 531.
22. L. L. MESHKOV, L. S. GUZEI and E. M. SOKOLOVSKAYA, *Russ. J. Phys. Chem.* **49** (1975) 1128.
23. I. KATAYAMA, H. SHIMATANI and Z. KOZUKA, *Nippon Kinzoku Gakkai Shi* **37** (1973) 509.
24. L. KAUFMAN and H. NESOR, *Calphad* **2** (1978) 59.
25. K. T. JACOB, *J. Mater. Sci.* **15** (1980) 2167.
26. W. H. McCARROLL, L. KARTZ and R. WARD, *J. Amer. Chem. Soc.* **79** (1957) 5410.
27. D. R. STULL and H. PROPHET, "JANAF Thermochemical Tables", NSRDS-NBS 37 (US Department of Commerce, Washington, DC, 1971).
28. K. T. JACOB, *J. Mater. Sci.* **12** (1977) 1647.
29. J. GHOSE, N. N. GREENWOOD, G. C. HALLAM and D. A. READ, *J. Solid State Chem.* **19** (1976) 365.
30. M. W. CHASE Jr, J. L. CURNUTT, J. R. DOWNEY Jr, R. A. McDONALD, A. N. SYVERUD and E. A. VALENZUELA, "JANAF Thermochemical Tables", 1982 Supplement, *J. Phys. Chem. Ref. Data* **11** (1982) 695.
31. L. KAUFMAN and H. NESOR, "Treaties on Solid State Chemistry", Vol. 5 (Plenum, New York, 1975) p. 179.
32. L. KAUFMAN, *Calphad* **1** (1977) 7.
33. A. PETRIC and K. T. JACOB, *Metall. Trans. A* **16A** (1985) 503.
34. K. T. JACOB and B. V. KUMAR, *Zeit. Metallkde* **77** (1986) 207.

Received 11 November 1986
and accepted 27 April 1987